



## **Influence of P<sub>2</sub>O<sub>5</sub> and Al<sub>2</sub>O<sub>3</sub> content on the structure of erbium-doped borosilicate glasses and on their physical, thermal, optical and luminescence properties**

Kevin Bourhis, Jonathan Massera, Laetitia Petit, Heikki Ihalainen, Alexandre Fargues, Thierry Cardinal, Leena Hupa, Mikko Hupa, Marc Dussauze, Vincent Rodriguez, et al.

### **► To cite this version:**

Kevin Bourhis, Jonathan Massera, Laetitia Petit, Heikki Ihalainen, Alexandre Fargues, et al.. Influence of P<sub>2</sub>O<sub>5</sub> and Al<sub>2</sub>O<sub>3</sub> content on the structure of erbium-doped borosilicate glasses and on their physical, thermal, optical and luminescence properties. Materials Research Bulletin, 2015, 63, pp.41-50. 10.1016/j.materresbull.2014.11.048 . hal-01091966

**HAL Id: hal-01091966**

**<https://hal.science/hal-01091966>**

Submitted on 14 Apr 2015

**HAL** is a multi-disciplinary open access archive for the deposit and dissemination of scientific research documents, whether they are published or not. The documents may come from teaching and research institutions in France or abroad, or from public or private research centers.

L'archive ouverte pluridisciplinaire **HAL**, est destinée au dépôt et à la diffusion de documents scientifiques de niveau recherche, publiés ou non, émanant des établissements d'enseignement et de recherche français ou étrangers, des laboratoires publics ou privés.

Influence of P<sub>2</sub>O<sub>5</sub> and Al<sub>2</sub>O<sub>3</sub> content on the structure of erbium-doped  
borosilicate glasses and on their physical, thermal, optical and  
luminescence properties

Kevin Bourhis<sup>a,\*</sup>, Jonathan Massera<sup>b</sup>, Laetitia Petit<sup>c</sup>, Heikki Ihalainen<sup>c</sup>, Alexandre Fargues<sup>d</sup>, Thierry  
Cardinal<sup>d</sup>, Leena Hupa<sup>b</sup>, Mikko Hupa<sup>b</sup>, Marc Dussauze<sup>e</sup>, Vincent Rodriguez<sup>e</sup>, Catherine Boussard-  
Plédel<sup>f</sup>, Bruno Bureau<sup>f</sup>, Claire Roiland<sup>f</sup> and Monica Ferraris<sup>a</sup>

<sup>a</sup>*Politecnico di Torino, DISAT, Istituto di Ingegneria e Fisica dei Materiali, Corso Duca degli  
Abruzzi 24, I-10129, Torino, Italy*

<sup>b</sup>*Process Chemistry Centre, Åbo Akademi University, Biskopsgatan 8, FI-20500, Turku, Finland*

<sup>c</sup>*nLIGHT Corporation, Sorronrinne 9, FI-08500 Lohja, Finland*

<sup>d</sup>*CNRS, Université de Bordeaux, ISM, 351 Cours de la Libération, F-33405 Talence, France*

<sup>e</sup>*CNRS, Université de Bordeaux, ICMCB, 87 Avenue du Dr Schweitzer, F-33608 Pessac, France*

<sup>f</sup>*Equipe Verres et Céramiques, UMR-CNRS 6226, Inst. des Sciences chimiques de Rennes,  
Université de Rennes 1, 35042 Rennes CEDEX, France*

\* Corresponding author. Tel.: +33 540163185. E-mail: [k.bourhis@argolight.com](mailto:k.bourhis@argolight.com) (K. Bourhis).

**Abstract**

The effect of P<sub>2</sub>O<sub>5</sub> and/or Al<sub>2</sub>O<sub>3</sub> addition in Er-doped borosilicate glasses on the physical,  
thermal, optical and luminescence properties is investigated. The changes in these glass properties  
are related to the glass structure modifications induced by the addition of P<sub>2</sub>O<sub>5</sub> and/or Al<sub>2</sub>O<sub>3</sub>, which  
were probed by FTIR, <sup>11</sup>B MAS NMR and X-ray photoelectron spectroscopies. Variations of the  
polymerization degree of the silicate tetrahedra and modifications in the <sup>[3]</sup>B/<sup>[4]</sup>B ratio are explained  
by a charge compensation mechanism due to the formation of AlO<sub>4</sub>, PO<sub>4</sub> groups and the formation  
of Al–O–P linkages in the glass network. From the absorption and luminescence properties of the

1 Er<sup>3+</sup> ions at 980 nm and 1530 nm, declustering is suspected for the highest P<sub>2</sub>O<sub>5</sub> concentrations  
2 while for the highest Al<sub>2</sub>O<sub>3</sub> concentrations no declustering is observed.

3

4 *Keywords:* A. Glasses; C. Infrared spectroscopy; C. Nuclear magnetic resonance (NMR); D. Optical  
5 properties; D. Luminescence

6

## 7 **1. Introduction**

8 Materials doped with rare-earth (RE) (e.g. Nd<sup>3+</sup>, Er<sup>3+</sup>, Yb<sup>3+</sup>, Tm<sup>3+</sup>) are of crucial importance  
9 in optoelectronics and are widely deployed in fiber amplifiers and solid-state lasers [1,2]. The  
10 coincidence between the Er<sup>3+</sup> emission band around 1530 nm and the principal low-loss window in  
11 the absorption spectrum of silicate-based optical fibers has been the main driving force behind  
12 much recent work on erbium-doped silica optical fibers and waveguides [2,3]. Intense efforts are  
13 on-going worldwide to increase the performances of the Er-doped silica-based fibers used as solid-  
14 state lasers and amplifiers. These performances are governed by the relevant electronic and optical  
15 characteristics of the active ion, such as absorption and emission cross sections, spectral shapes of  
16 the emission and absorption bands, excited state lifetimes, as well as the ion-ion interactions. The  
17 host material also has an important impact on all these properties [4,5]. Most of the work reported  
18 on Er<sup>3+</sup>-doped fiber lasers and amplifiers has used high silica-content glasses co-doped with various  
19 combinations of Ge, P, and Al atoms [2,3,5]. The main limitations of Er-doped silicate fibers  
20 originate from the low solubility of the erbium ions resulting in the formation of Er–Er clusters for  
21 the highest erbium concentrations. Er–Er energy transfers most often result in the non-radiative  
22 relaxation of the ion pair leading to a quenching of the luminescence at high erbium contents. To  
23 prevent such clustering, the fiber core can be additionally doped with alumina or phosphorus  
24 pentoxide [6]. It was shown that silica-based glasses should contain at least 8-10 Al or 15 P atoms  
25 per rare-earth ion (mainly Yb<sup>3+</sup> and Nd<sup>3+</sup>) to prevent RE clustering [7–10]. Moreover, these oxides

1 have also a significant impact on the silica network [11]. Du *et al.* showed that the introduction of  
2 aluminum cations in sodium silicate glasses leads to the formation of negatively-charged  $[Al\emptyset_4]^-$   
3 groups, where  $\emptyset$  denotes a bridging-oxygen (bO) atom [12]. A charge compensation mechanism  
4 occurs within the glass structure resulting in the transformation of the silicate units with non-  
5 bridging oxygen atoms (noted Si-nbO) into units with bridging oxygen atoms (noted Si-bO). The  
6  $Na^+$  ions, previously neutralizing the Si-nbO atoms, are transferred to the  $[Al\emptyset_4]^-$  tetrahedra [12,13].  
7 In  $Na_2O-B_2O_3-SiO_2$  (NBS) glasses the charge excess is preferentially compensated by the borate  
8 groups and in a lesser extent by the silicate groups, as evidenced by IR [12-17] and NMR  
9 spectroscopies [12,18].

10 Co-doping silica glass simultaneously with  $Al_2O_3$  and  $P_2O_5$  presents an interesting  
11 cooperative behavior. Likhachev *et al.* showed that the rare-earth dissolution in the ternary  
12  $Al_2O_3-P_2O_5-SiO_2$  host systems was higher than in the binary  $P_2O_5-SiO_2$  or  $Al_2O_3-SiO_2$  glasses  
13 [19]. Although doping with  $Al_2O_3$  or  $P_2O_5$  increases the refractive index (RI) of silica glasses, co-  
14 doping the silica glass with  $Al_2O_3$  and  $P_2O_5$  leads to the formation of a glass with a lower RI than  
15 that of silica, that the authors related to the formation of  $AlPO_4$ -like units in the glass network  
16 [6,20,21]. The authors stated that such units are created at the expense of  $[P\emptyset_4]^-$  and  $[Al\emptyset_4]^-$  units,  
17 resulting in the formation of Al–O–P linkages with similar bond strength than those in Si–O–Si  
18 linkages [20]. This offers the possibility of doping the glass with higher concentrations of  $P_2O_5$  and  
19  $Al_2O_3$  to improve the RE dissolution, thus limiting the RE clustering in the fiber while maintaining  
20 a low refractive index. To the best of our knowledge, there have been very few studies on the  
21 influence of  $P_2O_5$  and  $Al_2O_3$  on the properties of glasses with a low silica-content.

22 In this paper, erbium-doped sodium-borosilicate glasses with different  $Al_2O_3/P_2O_5$  ratios  
23 have been prepared to better understand the role of  $P_2O_5$  and  $Al_2O_3$  on the  $Er^{3+}$  emission properties.  
24 The main parameters affecting the luminescence at 1530 nm (absorption properties at 980 nm and

1530 nm, concentration of hydroxyl groups) have been investigated and related to structural modifications of the glass network induced by the introduction of  $P_2O_5$  and/or  $Al_2O_3$ .

## 2. Experimental

### 2.1 Sample preparation

Glasses having the composition  $50SiO_2-21.82Na_2O-28.06B_2O_3-0.12Er_2O_3$  (matrix) and  $50SiO_2-20.51Na_2O-26.36B_2O_3-0.12Er_2O_3-xAl_2O_3-(3-x)P_2O_5$  ( $x = 0-3$  mol%) were prepared using  $NaH_2PO_4 \cdot H_2O$  (Merck, 99%),  $H_3BO_3$  (Aldrich, 99.99%),  $Na_2CO_3$  (Sigma-Aldrich, >99.5%),  $Al_2O_3$  (Sigma-Aldrich, >99%),  $SiO_2$  (Sigma-Aldrich, 99%),  $Er_2O_3$  (MV Laboratory, 99.999%) as raw materials in powder form. For the P/Al co-doped glasses, a fraction of the  $B_2O_3$  and  $Na_2O$  content is substituted by  $P_2O_5$  and/or  $Al_2O_3$ . The compositions of the studied glasses are listed in Table 1. Before melting, the batches were treated at 400 °C for 15 h to completely decompose the raw materials. The batches were then melted in ambient atmosphere in alumina crucibles for 30 min between 1425°C and 1475°C, depending on the glass composition. After quenching on a brass mold, the glasses were annealed for 3 h at 40°C below their respective glass transition temperature ( $T_g$ ) to remove the internal stress. Finally the samples were cut, ground and polished. The glass compositions were checked by electron-probe micro-analysis and were found to be in accordance with the theoretical ones, within the accuracy of measurement ( $\sim 0.1$  wt%). The  $Er^{3+}$  concentration is almost the same in all glasses except for the glass matrix for which it is slightly higher.

### 2.2 Optical measurements

A fully automated Metricon, model 2010 prism-coupled refractometer was used to measure the refractive indices (RI) at 1312 nm,  $n^{1312}$ . The accuracy of the measurement is estimated to be  $\pm 0.003$ . Each measurement was repeated 5 times and at least 3 measurements were performed on different areas of the glass. When the standard deviation (SD) of the measurements was superior to 0.003, the SD was used as uncertainty.

The UV-Vis-NIR absorption spectra were measured on 2 mm-thick samples with a double-beam spectrophotometer (CARY 5000 UV-VIS-NIR) over the 250-2500 nm spectral region. The absorption spectra over the 2500-4000  $\text{cm}^{-1}$  range were performed on a FTIR Bruker Alpha-T spectrometer with a spectral resolution of 2  $\text{cm}^{-1}$ . The measurements were performed at room temperature and were corrected for the Fresnel losses, which are estimated to be about 7.73-7.67% at 1312 nm (extreme RI values = 1.502 and 1.493). The absorption cross-sections,  $\sigma_{\text{abs}}(\lambda)$ , were calculated from the absorption spectra using Equation (1).

$$\sigma_{\text{abs}}(\lambda) = 2.303 \times \log(I_0/I) / (NL) = \alpha(\lambda) / L, \quad (1)$$

where  $\log(I_0/I)$  is the absorbance,  $N$  the rare earth ion concentration,  $L$  the thickness of the sample and  $\alpha_{\text{abs}}(\lambda)$  the absorption coefficient.

### 2.3 Thermal and physical measurements

The glass transition ( $T_g$ ) and glass crystallization ( $T_x$ ) temperatures were measured by differential thermal analysis (Mettler Toledo TGA/SDTA851) at a heating rate of  $15^\circ\text{C}.\text{min}^{-1}$ . The  $T_g$  was taken at the inflection point of the endotherm, as obtained by taking the first derivative of the DSC curve. The  $T_g$  was determined with an accuracy of  $2^\circ\text{C}$ . The  $T_x$  was taken at the maximum point of the exotherm point. The  $T_x$  was determined with an accuracy of  $5^\circ\text{C}$ , and was hardly or not distinguishable in some cases.

The density of the bulk glasses was measured after Archimedes' method in distilled water as an immersion fluid. The accuracy was better than 0.3 %.

### 2.4 Luminescence measurements

The emission spectra in the 1400–1700 nm range were measured at room temperature using an AOC (Applied Optronics Corp.) laser diode excitation source emitting at 980 nm, an Edinburgh Instruments monochromator (M300) and a liquid nitrogen cooled germanium detector (ADC 403L).

1 The emission spectra of the samples were collected on powder between quartz plates to avoid  
2 reabsorption.

3

#### 4 *2.5 Infrared spectra measurements*

5 The reflexion infrared spectra were obtained using a Fourier-transform spectrometer  
6 (Nicolet 6700 FTIR), by utilizing a 12° off-normal reflection attachment and a high-reflectivity  
7 mirror as reference. A proper combination of DTGS detector and beam-splitters (germanium-coated  
8 KBr beam splitter or hybrid FIR beam splitter) allowed the measurement of continuous reflectance  
9 spectra in the 100–7000 cm<sup>-1</sup> range. Each spectrum represents the average of 200 scans at 1 cm<sup>-1</sup>  
10 resolution. The spectrometer was purged with dry air to minimize atmospheric CO<sub>2</sub> and water  
11 vapor. The reflectance data were analyzed by the Kramers–Krönig transformation to obtain  
12 frequency-dependent phase angle between reflected and incident wave. The reflectivity and phase  
13 angle spectra were subsequently employed to calculate the optical and dielectric properties of  
14 glasses [22]. Infrared data reported in this work are in the form of the absorption coefficient spectra,  
15  $\alpha$ , calculated from the relation,

$$16 \quad \alpha = 4 \pi \nu k = 2 \pi \nu \varepsilon'' / n, \quad (2)$$

17 where  $n$  and  $k$  are the frequency-dependent real and imaginary parts of the refractive index,  
18 respectively,  $\varepsilon''$  is the imaginary part of the dielectric constant and  $\nu$  is the frequency.

19

#### 20 *2.6 XPS spectra measurements*

21 The X-ray photoelectron spectra were obtained using a PHI 5000 VersaProbe (PHI  
22 Electronics) spectrometer. Monochromatic Al K $\alpha$  radiation (1486.6 eV) was operated under a  
23 residual pressure of 5×10<sup>-9</sup> mbar. The spectrometer was calibrated using the photoemission lines of  
24 Au (Au 4f<sub>7/2</sub> = 83.9 eV, with reference to the Fermi level). Survey spectra were recorded from 0 to  
25 1400 eV with a pass energy of 187.5 eV using 1 eV steps and four scans. High resolution spectra of

the O1s, C1s and Si2p bands were recorded with a pass energy of 23.50 eV. Scan accumulation enabled to reach a satisfactory signal/noise ratio. Binding energies have been corrected using adventitious hydrocarbon carbon (C1s peak at 284.8 eV) as a reference.

## 2.7 $^{11}\text{B}$ MAS NMR measurements

Solid State  $^{11}\text{B}$  MAS NMR experiments were carried out with a Bruker Avance 600 spectrometer working at 192 MHz for  $^{11}\text{B}$ . The spectra were acquired under magic angle spinning (MAS) at a spinning rate of 30 kHz using a 2.5 mm diameter rotor. A 50 kHz radio-frequency field was used for excitation, ensuring an homogeneous and selective excitation of the central transition. A spin echo sequence was used, synchronized on the spinning speed, in order to avoid probe signal and distortion of the baseline. Thus, the delay between two pulses was 33  $\mu\text{s}$ . Besides, it is known that both boron families, the  $^{31}\text{B}$  and  $^{41}\text{B}$  contributions, have different transverse relaxation times ( $T_2$ ). In order to get some quantitative results, the  $T_2$  were properly measured,  $T_2(^{31}\text{B}) = 16$  ms, and  $T_2(^{41}\text{B}) = 10$  ms, and the integrated intensities of each component were corrected following the equation  $I_0 = I(t) \cdot \exp(t/T_2)$ . The chemical shift scale was calibrated with respect to a 1 M  $\text{B}_2\text{O}_3$  solution. The spectra were reconstructed using the DMFIT software. The model chosen takes into account the spinning sidebands.

## 2.8 The Dell-Bray-Xiao model

The structure of alkaline borosilicate glasses can be described by the Dell, Bray and Xiao (DBX) model as described in [23]. Using the molar ratios  $R = \text{SiO}_2/\text{B}_2\text{O}_3$  and  $K = \text{Na}_2\text{O}/\text{B}_2\text{O}_3$ , this model is used to find the fractions of three ( $N_3$ ) and four ( $N_4$ ) coordinated boron in each glass after Equations 3–6.

- For  $0 \leq R \leq 0.5$   $\text{Na}_2\text{O}$  converts symmetrical trigonal  $^{31}\text{B}$  into diborate  $^{41}\text{B}$  units. In this range,  $N_4$  is given by

$$N_4 = R \quad (3)$$



- For  $0.5 \leq R \leq R_{\max}$  (where  $R_{\max} = 1/2 + K/16$ ), a borosilicate network starts to form. Additional  $\text{Na}_2\text{O}$  in excess of  $R = 0.5$  is used to destroy diborate groups and creates four loose  $^{[4]}\text{B}$  units per diborate. Every  $^{[4]}\text{B}$  unit is then bonded to four  $\text{Q}^4$  tetrahedra to form a reedmergnerite ( $1/2(\text{Na}_2\text{O} \cdot \text{B}_2\text{O}_3 \cdot 8\text{SiO}_2)$ ) group. In this range,  $N_4$  is given by

$$N_4 = R \quad (4)$$

- For  $R_{\max} \leq R \leq R_{d1}$  (where  $R_{d1} = 1/2 + K/4$ ),  $N_4$  is considered as constant and independent of the  $\text{Na}_2\text{O}$  content. The model assumes that all  $\text{Na}_2\text{O}$  in excess of  $R_{\max}$  are absorbed by reedmergnerite ( $1/2(\text{Na}_2\text{O} \cdot \text{B}_2\text{O}_3 \cdot 8\text{SiO}_2)$ ) groups and form nbO atoms on the silicate tetrahedra.  $N_4$  is given by

$$N_4 = R_{\max} \quad (5)$$

Note that for all values of  $R$ ,  $N_3$  is given by

$$N_3 = 1 - N_4 \quad (6)$$

In  $\text{P}_2\text{O}_5$ -NBS glasses,  $\text{P}_2\text{O}_5$  is expected to be mainly under the form of  $[\text{P}\text{O}_3\text{O}]^0$  tetrahedra (no pyrophosphate or  $\text{P}-\text{O}-\text{P}$  linkage), in analogy with phosphosilicate glasses given the low  $\text{P}_2\text{O}_5$  fraction (max. 3 mol%) [24]. In  $\text{Al}_2\text{O}_3$ -containing glasses, aluminum oxide has priority to associate itself with an equivalent amount of  $\text{Na}_2\text{O}$  to form  $[\text{Al}\text{O}_4]^-$  tetrahedra [13–15,25]. The excess  $\text{Na}_2\text{O}$  first associates with borate, as explained above, then with  $\text{SiO}_2$  by forming non-bridging oxygen atoms on the  $\text{Q}^4$  units. The  $N_4$  values can be estimated by the  $R'$  parameter, obtained by modifying the  $R$  parameter as follows:

$$N_4 = R' = (\text{Na}_2\text{O} - \text{Al}_2\text{O}_3) / \text{B}_2\text{O}_3 (= R'_{\max}) \quad (7)$$

The  $\text{Q}^3$  and  $\text{Q}^4$  silicate units proportion can thus be calculated from Equation 7:

$$\text{Q}^3 = (\text{SiO}_2 - 2\text{Na}_2\text{O}^{\text{exc}}) / \text{SiO}_2; \text{Q}^4 = 1 - \text{Q}^3 \quad (8)$$

where  $\text{Na}_2\text{O}^{\text{exc}}$  is defined as  $\text{Na}_2\text{O} - (\text{Al}_2\text{O}_3 + 2R'_{\max} \times \text{B}_2\text{O}_3)$

### 3. Results

#### 3.1. Physical properties

The evolutions of the refractive index at 1312 nm and of the glass transition temperature as a function of  $x$  are shown in Fig. 1a and 1b, respectively. The addition of  $P_2O_5$  ( $x = 0$ ) or  $Al_2O_3$  ( $x = 3$ ) in the glass matrix leads to a decrease of the refractive index. The error bar for  $x = 0$  is quite large since a wide dispersion of the refractive index values was observed for this composition. It can be related to the low solubility of  $P_2O_5$  in silicate-based glasses in agreement with [26]. The refractive index can be considered as almost constant on the composition range, with slightly higher values for  $x$  close to 1.5.

The  $T_g$  for  $x = 0$  is lowered while it is almost equal to the matrix one for  $x = 3$ . A continuous increase of the  $T_g$  can be seen when  $x$  increases from 0 to 3. The difference ( $T_x - T_g$ ) is presented in the inset of Fig. 1b. For the matrix glass, no crystallization peak was detected. The presence of  $P_2O_5$  ( $x = 0$ ) or  $Al_2O_3$  ( $x = 3$ ) gives rise to a maximum of ( $T_x - T_g$ ) at around 260 °C and 220 °C, respectively. This difference progressively decreases between  $x = 0$  and 3 and reaches a local minimum at around 110 °C for  $x = 1.67$ .

#### 3.2. UV-Vis-NIR absorption spectra

A typical absorption spectrum in the UV-Vis-Near IR range of an  $Er^{3+}$ -doped glass (matrix) is depicted in Fig. 2a. We found that the UV absorption edge is not clearly affected by  $x$  and that the cut-off wavelength remains almost constant at  $\sim 315$  nm. In the 250–1600 nm range, several bands characteristic of the  $Er^{3+}$  ion transitions from the ground state to various excited levels are observed. The absorption bands at 980 nm and 1530 nm are represented in Fig. 2b and 2c, respectively. The shape of the band at 980 nm (inset of Fig. 2b) remains almost unchanged while some modifications are observed at 1490 nm and 1530 nm (inset of Fig. 2c) with the addition of  $P_2O_5$  and/or  $Al_2O_3$ . The spectral bandwidth is almost constant in both cases (21–23 nm at 980 nm and 24–26 nm at 1530 nm). The evolution of the absorption cross-sections at 980 nm,  $\sigma_{abs}(980)$ , and of the integrated area

at 1530 nm,  $A^{\text{Abs}}(1530)$ , are plotted respectively in Fig 2d and 2e, respectively. They have very similar evolutions: the introduction of  $\text{P}_2\text{O}_5$  ( $x = 0$ ) increases  $\sigma(980)$  and  $A^{\text{Abs}}(1530)$  while these values are similar to the matrix ones when  $\text{Al}_2\text{O}_3$  ( $x = 3$ ) is introduced. Both  $\sigma_{\text{abs}}(980)$  and  $A^{\text{Abs}}(1530)$  decrease when  $x$  increases from 0 to 3. A slight increase of these values is noticed for  $x \sim 1.5$ .

The absorption spectra recorded between 3000 and 4000  $\text{cm}^{-1}$  are reported in Fig. 3 for some glasses (matrix,  $x = 0, 1.5$  and 3). The spectra show a broad absorption band peaking at around 3500  $\text{cm}^{-1}$  usually attributed to OH groups in several oxide glasses [27]. The free OH content can be estimated from the absorption coefficient at 3500  $\text{cm}^{-1}$ ,  $\alpha$ , using Eq. 9

$$[\text{OH}] = \alpha \times N_A / \varepsilon, \quad (9)$$

where  $N_A$  is the Avogadro constant and  $\varepsilon$  is the molar absorptivity of the free OH groups in the glass, taken equal to  $\varepsilon = 49.1 \times 10^3 \text{ cm}^2/\text{mol}$  [28].

The values of  $\alpha$  and  $[\text{OH}]$  for the different glass compositions are listed in Table 1. They are comparable to those reported in several silicate glasses [29,30].  $[\text{OH}]$  is close to  $5\text{--}6 \times 10^{19} \text{ ions.cm}^{-3}$  for most of the glasses, with slightly higher values for the glasses with  $x = 0.5$  and 1. It has to be noted that  $[\text{OH}]$  in the P/Al-doped glasses is higher to the one of the matrix glass.

### 3.3. Luminescence properties

The emission spectra after excitation at 980 nm for some glasses (matrix,  $x = 0, 1.5$  and 3) are depicted in Fig. 4a. They arise from the  $^4\text{I}_{13/2} \rightarrow ^4\text{I}_{15/2}$  transition typical of the  $\text{Er}^{3+}$  emission in oxide glasses. As seen for the absorption bands at 1530 nm, the shape of the emission bands depends on the glass composition. The spectral bandwidth remains almost constant upon the composition modification (32-35 nm). The changes in the shape of the emission band (inset of Fig. 4a) were found to be more pronounced in the case of the glasses with  $0 \leq x \leq 1.5$ . Fig. 4b presents

1 the variation of the integrated area of the emission band at 1530 nm,  $A^{\text{Em}}(1530)$ , as a function of  $x$ .  
2  $A^{\text{Em}}(1530)$  has a similar evolution as  $\sigma(980)$  and  $A^{\text{Abs}}(1530)$ .  $A^{\text{Em}}(1530)$  strongly decreases when  $x$   
3 increases, with a local minimum at  $x \sim 1.5$ . The glasses with  $x \leq 1$  exhibit a larger emission  
4 intensity at 1530 nm than the matrix glass, whereas the glasses with  $x > 2$  exhibit a lower emission  
5 intensity.

### 7 3.4. Structural characterization

8 The IR spectra in the 250-1600  $\text{cm}^{-1}$  range are depicted in Fig. 5a-c. The spectra are  
9 composed of broad bands situated in the 400–700, 800–1200  $\text{cm}^{-1}$  and 1200–1500  $\text{cm}^{-1}$  ranges. The  
10 spectra are dominated by an intense band at 1030  $\text{cm}^{-1}$  accompanied by shoulders near 900  $\text{cm}^{-1}$  and  
11 1150  $\text{cm}^{-1}$ . The high-frequency domain exhibits two bands at 1290  $\text{cm}^{-1}$  and 1385  $\text{cm}^{-1}$  with a  
12 shoulder at around 1470  $\text{cm}^{-1}$ . In the low-frequency part, a rather intense band at 450  $\text{cm}^{-1}$  and a less  
13 intense one at around 710  $\text{cm}^{-1}$  are visible. As seen in Fig. 5a, the introduction of  $\text{P}_2\text{O}_5/\text{Al}_2\text{O}_3$  ( $x = 0$   
14 or 3) in the matrix glass strongly modifies the spectra. Though the position of the most intense band  
15 at 1030  $\text{cm}^{-1}$  is not significantly affected by the compositional modifications, its width slightly  
16 increases on both low- and high-frequency sides. The intensity of the bands in the 1200–1600  $\text{cm}^{-1}$   
17 range decreases depending on the glass composition, a minimum amplitude of these bands being  
18 observed for the glass with  $x = 0$ . In the low frequency part, the intensity of the bands at 450 and  
19 710  $\text{cm}^{-1}$  increases, the band at 450  $\text{cm}^{-1}$  also becomes sharper for the  $\text{P}_2\text{O}_5/\text{Al}_2\text{O}_3$ -containing  
20 glasses compared to that of the matrix. The intensity of the bands of the glass for  $x = 1.5$  are  
21 intermediate between the ones of the -matrix glass and the ones of the  $\text{P}_2\text{O}_5/\text{Al}_2\text{O}_3$ -containing  
22 glasses.

23 Comparable evolutions are noticed when  $x$  increases from 0 to 1.5 and when  $x$  decreases from 3 to  
24 1.5. When  $x$  increases from 0 to 1.5 or decreases from 3 to 1.5, a widening of the main band at 1030  
25  $\text{cm}^{-1}$  is observed when approaching the composition  $x = 1.5$  for which the molar ratio  $\text{Al}/\text{P} = 1$ . The

intensity of the bands in the range 1200–1600  $\text{cm}^{-1}$  increases while the amplitude of the bands at 450  $\text{cm}^{-1}$  and 710  $\text{cm}^{-1}$  slightly decreases when  $x$  increases from 0 to 1.5 and when  $x$  decreases from 3 to 1.5 (which is less evident for the band at 710  $\text{cm}^{-1}$ ). It has to be noted that the maximum of the band at 450  $\text{cm}^{-1}$  is shifted to higher wavenumbers when  $x$  comes close to 1.5.

Fig. 6a presents the Si2p XPS spectra of some glasses (matrix,  $x = 0, 1.5$  and 3). The Si2p spectrum of the glass matrix is composed of a wide band peaking at  $\sim 102.8$  eV. The addition of  $\text{P}_2\text{O}_5$  ( $x = 0$ ) and/or  $\text{Al}_2\text{O}_3$  ( $x = 3$ ) leads to a shift of the band to higher binding energy (BE). Fig. 6b represents the evolution of the Si2p band maximum as a function of  $x$ . When  $x$  increases from 0 to 1, the position of the Si2p remains almost constant, then shifts to lower BE when  $x$  increases up to 1.67. When  $x$  further increases from 1.67 to 3, the Si2p band shifts to higher BE.

The  $^{11}\text{B}$  MAS-NMR spectra of some glasses (matrix,  $x = 0, 1.5$  and 3) are presented in Fig. 7a. The two peaks centered at 12 and -1 ppm are attributed to  $^{[3]}\text{B}$  and  $^{[4]}\text{B}$ , respectively, in agreement with [18,31]. The relative values for both sites as a function of  $x$  are presented in Fig. 7b. The  $^{[4]}\text{B}$  fraction reaches its highest value (60%) for  $x = 0$ , decreases to 53% when  $x$  increases from 0 to 1.5 (close to the level of the matrix glass) and finally increases when  $x$  increases from 1.5 to 3.

The three ( $\text{N}_3$ ) and four ( $\text{N}_4$ ) coordinated boron were estimated using the Dell-Bray-Xiao model as explained in the experimental section. Table 2 lists the  $\text{N}_4$ ,  $\text{N}_3$ ,  $\text{Q}_4$  and  $\text{Q}_3$  proportion calculated according to the Dell-Bray-Xiao model. Since  $R_{\text{max}} \leq R' \leq R_{\text{dl}}$ , the  $^{[4]}\text{B}$  fraction is expected to be a constant which is in disagreement with the measurement. The DBX model also predicts that the  $\text{Q}^4$  fraction increases linearly when  $x$  increases (see Fig. 8).

#### 4. Discussion

#### 1    4.1. Evolution of the refractive index and of the glass transition temperature

2            The refractive index depends on the overall polarizability of the glass matrix. P and Al are  
3    less polarizable than Na. Therefore the observed decrease of refractive index might be due to the  
4    partial replacement of Na<sub>2</sub>O by P<sub>2</sub>O<sub>5</sub> or Al<sub>2</sub>O<sub>3</sub>.

5            The lower  $T_g$  for  $x = 0$  than for  $x = 3$  can be explained by the number of bonding oxygen  
6    atoms born by the P or Al atoms. When P<sub>2</sub>O<sub>5</sub> is introduced in the glass ( $x = 0$ ) [PØ<sub>3</sub>O]<sup>0</sup> units are  
7    formed, whereas when Al<sub>2</sub>O<sub>3</sub> is introduced in the glass ( $x = 3$ ) [AlØ<sub>4</sub>]<sup>-</sup> groups are formed. The 3-  
8    bonded [PØ<sub>3</sub>O]<sup>0</sup> units, with one terminal atom, weaken the network compared to the 4-bonded  
9    [AlØ<sub>4</sub>]<sup>-</sup> units, giving rise to a glass with a higher  $T_g$  for  $x = 3$

10

#### 11    4.2. Evolution of the glass structure as a function of $x$

12            The structure of sodium-borosilicate glasses is generally described as mixed silicate and  
13    borate networks [18,32–37]. Borate groups appear to exist largely as polymerized trigonal [<sup>3</sup>B] and  
14    tetragonal ([<sup>4</sup>B]) units and silicate units as tetrahedral SiO<sub>4</sub> units (Q<sup>n</sup>), where n is the number of bO  
15    atoms [12,17,38–42].

16    In the IR spectrum of the glass matrix (Fig. 5a), the main band at 1030 cm<sup>-1</sup> is associated to the  
17    Si–O asymmetric stretching vibrations of the Q<sup>n</sup> groups, superposed with the asymmetric stretching  
18    vibrational modes of Si–O–B and B–O–B bridges at around 1080 cm<sup>-1</sup> and 1250 cm<sup>-1</sup>  
19    [33,35,40–44]. The shoulder in the 900-1000 cm<sup>-1</sup> range is related to the symmetric stretching of the  
20    Si–O–[<sup>4</sup>B] and [<sup>3</sup>B]–O–[<sup>4</sup>B] vibrations modes superposed to the asymmetric stretching of the [BØ<sub>4</sub>]<sup>-</sup>  
21    tetrahedra [16,40–42,44,45]. The two bands at 1270 cm<sup>-1</sup>, 1385 cm<sup>-1</sup> and the shoulder at 1470 cm<sup>-1</sup>  
22    are related to the asymmetric stretching vibrations of various [<sup>3</sup>B] units in different ring and non-  
23    ring configurations [13,34,35,42,45]. The band of low intensity at 710 cm<sup>-1</sup> is related to the bending  
24    modes of the Si–O–Si, Si–O–B and B–O–B linkages and can be superposed to the bending  
25    vibrations of [<sup>3</sup>B] units [13,22,34]. The low-frequency envelope in the 400–550 cm<sup>-1</sup> arises from the

1 rocking motion of Si–O–Si linkages as well as deformation modes of various borate species  
 2 [13,22,35,45,46]. The introduction of P<sub>2</sub>O<sub>5</sub> (x = 0) or Al<sub>2</sub>O<sub>3</sub> (x = 3) in the glass matrix leads to the  
 3 formation of [PØ<sub>3</sub>O]<sup>0</sup> and [AlØ<sub>4</sub>]<sup>–</sup> units, which present typical absorption bands at ~ 970 cm<sup>–1</sup> [47]  
 4 and at ~ 900 cm<sup>–1</sup> [13], respectively, corresponding to the vibrations of the Si–O–(Al,P) linkages.  
 5 Given the low P<sub>2</sub>O<sub>5</sub> fraction (max. 3 mol%), phosphate atoms are expected to be mainly under the  
 6 form of [PØ<sub>3</sub>O]<sup>0</sup> tetrahedra (no pyrophosphate or P–O–P linkage), in analogy with phosphosilicate  
 7 glasses [24]. The introduction of such units have an impact on the structure of the glass: the addition  
 8 of P<sub>2</sub>O<sub>5</sub> or Al<sub>2</sub>O<sub>3</sub> at the expense of Na<sub>2</sub>O and B<sub>2</sub>O<sub>3</sub> leads to a glass network with a larger amount of  
 9 bO atoms on the silicate groups than in the glass matrix as suspected from the shift of the Si2p BE  
 10 band to higher energy which is in agreement with the Dell-Bray-Xiao model (See Fig. 8). One can  
 11 notice that the addition of P<sub>2</sub>O<sub>5</sub> or Al<sub>2</sub>O<sub>3</sub> also leads to an increase in <sup>[4]</sup>B (Fig. 7b). As explained in  
 12 [12–16,18], these changes in the glass structure are suspected to be related to a charge  
 13 compensation mechanism taking place to neutralize the negative charges of the [AlØ<sub>4</sub>]<sup>–</sup> units. These  
 14 changes in the glass network result in a larger amount of OH groups as shown in Fig. 3  
 15 When x increases from 0 to 1.5 or decreases from 3 to 1.5, the Si2p band shifts to lower BE  
 16 indicating the formation of a less polymerized silicate network. This hypothesis is also comforted  
 17 by the shift of the IR band at 470 cm<sup>–1</sup> when x increases from 0 to 1.5 or decreases from 3 to 1.5. It  
 18 also leads to a decrease in <sup>[4]</sup>B (Fig. 7b).

19 These changes in the glass structure are not in agreement with the evolutions predicted by  
 20 the Dell-Bray-Xiao model. The Q<sup>4</sup> fraction is expected to increase linearly as illustrated in Fig. 8  
 21 and N<sub>4</sub> are supposed to be x independent in disagreement with our measurements. The discrepancy  
 22 between the prediction of the DBS model and our results, can be explained by the fact that P<sub>2</sub>O<sub>5</sub> not  
 23 only leads to tri-bonded [PØ<sub>3</sub>O]<sup>0</sup> units but also to charged [PØ<sub>2</sub>O<sub>2</sub>]<sup>–</sup> units. Such units thus have the  
 24 same behavior as [AlØ<sub>4</sub>]<sup>–</sup> units and also need to be charge-compensated when present in the glass.  
 25 Assuming that the P<sub>2</sub>O<sub>5</sub> is only present under the form of [PØ<sub>2</sub>O<sub>2</sub>]<sup>–</sup> units, the amount of negatively-

1 charged units brought by  $P_2O_5$  and  $Al_2O_3$  is similar independently for  $x = 0$  or 3. However the  
 2 presence probability of such units in the glass is low. Several authors reported the formation of  
 3  $AlPO_4$  structural units when  $P_2O_5$  and  $Al_2O_3$  are introduced in pure silica glass network. The pure  
 4  $AlPO_4$  crystal consists of a  $[PO_4^{3-}]$  network isolated by  $Al^{3+}$  cations [48,49]. The presence of such  
 5 units in the glass network was suspected due to an improvement of the optical properties such as  
 6 fluorescence enhancement or the decrease of the refractive index of the glass [6,8,11]. Here, the  
 7  $P_2O_5$ - and  $Al_2O_3$ -containing glass networks are suspected to contain simple isolated Al–O–P  
 8 linkages rather than crystalline  $AlPO_4$  units. Such units exhibit infrared absorption bands located at  
 9  $730\text{ cm}^{-1}$  and at  $1130\text{ cm}^{-1}$  according to [48,49], which eventually contribute to the appearance and  
 10 increase in intensity of shoulders on both sides of the main absorption band (Fig. 5). Since Al–O–P  
 11 linkages in  $AlPO_4$  units have similar bond strengths than the  $SiO_4$  units [20] their presence in the  
 12 glass network is expect to lead to a small increase in  $T_g$  (Fig. 1b). It is also supported by the strong  
 13 decrease in the  $(T_x - T_g)$  difference at around  $x \sim 1.5$  (Inset of Fig. 1b), indicating the high tendency  
 14 of the glass  $x=1.5$  to crystallization that may be due to a higher number of Al–O–P linkages.

15 The DBX model was modified to take into account the formation of such linkages by  
 16 simulating the formation of  $AlPO_4$  units. In this hypothesis the simultaneous presence of  $Al_2O_3$  and  
 17  $P_2O_5$  leads to the formation of two  $AlPO_4$  units, so that there is one more  $Na_2O$  free to interact with  
 18 the borosilicate network. Therefore,  $R^*$ , defined in Equation 8, can be modified as follows:

$$19 \quad R^* = (Na_2O - Al_2O_3 - P_2O_5 + 2 \times AlPO_4) / B_2O_3 \quad (10)$$

20 The  $Q^3$  and  $Q^4$  silicate units proportion can thus be calculated from Equation 11:

$$21 \quad Q^3 = (SiO_2 - 2Na_2O^{exc}) / SiO_2 = 2 \times (R^* - R_{max}) / K; \quad Q^4 = 1 - Q^3 \quad (11)$$

22 It can be seen in Fig. 8 that the modified DBX model simulating the formation of  $AlPO_4$  groups  
 23 shows modification of the silicate network evidenced by XPS spectroscopy, but is able neither to  
 24 give a quantitative analysis of the  $Q^n$  group distribution nor a good description of the borate network  
 25 changes induced by the increase of  $x$ . Because phase separation can exist between the borate and



1 the silicate network at the microscopic scale, it is possible to think that  $P_2O_5$  and/or  $Al_2O_3$  enter  
2 preferentially in the silicate or in the borate network, giving rise to discrepancies between the  
3 measured and predicted structure.

4  $Na^+$ ,  $[P\emptyset_4]^0$  and  $[Al\emptyset_4]^-$  not only act on the silicate network, as predicted by Dell and co-workers,  
5 but also on the borate network.

6 The two  $^{[3]}B$  and  $^{[4]}B$  coordinations can be combined to form different groups like boroxol  
7 rings, orthoborate, pentaborate, tetraborate, metaborate and diborate groups, etc. The  $^{[4]}B$  units give  
8 rise to tetrahedral network features in the glass structure, where  $BO_4$  units are always negatively  
9 charged ( $[B\emptyset_4]^-$ ), whereas  $^{[3]}B$  units may be present as neutral  $[B\emptyset_3]^0$ , charged units  $[B\emptyset_2O]^-$ ,  
10  $[B\emptyset O_2]^{2-}$  or even  $[BO_3]^{2-}$  [50].

11  $P_2O_5$  has been assumed to form only neutral  $[P\emptyset_4]^0$  units, so that the number of nbO in the glass  
12 should be unchanged for the matrix glass and for  $x = 0$ . Since an increase of the Si BE and of the  
13  $^{[4]}B$  content is observed, it is possible to conclude that some part of the nbO atoms born by the  
14 silicate network is transferred to the borate network. A fraction of  $^{[3]}B$  units may thus be present as  
15 charged  $[B\emptyset_2O]^-$  (metaborate) units. Given the large variation in the  $^{[4]}B$  fraction, it seems  
16 reasonable to suggest that phosphate groups enters preferentially the borate network. One cannot  
17 exclude the formation of  $[P\emptyset_3O]^-$  units requiring  $Na^+$  ions for charge compensation, which would  
18 slightly increase the amount of nbO atoms.

19 On the aluminate-rich side for  $x = 3$ , the  $[Al\emptyset_4]^-$  groups formed when  $Al_2O_3$  is introduced are  
20 charge-compensated by some  $Na^+$  ions, leading to a higher amount of bO atoms in the glass  
21 network. The slight increase of  $^{[4]}B$  fraction compared to the large XPS shift to high BE may  
22 indicate that the created bO atoms are born in a large extent by the silicate network, and in a lesser  
23 extent by the  $^{[3]}B$  units under the form of neutral  $[B\emptyset_3]^0$  units.

24 When  $P_2O_5$  and  $Al_2O_3$  are mixed the silicate network is depolymerized as indicated by the  
25 downshift of the Si BE, while the equilibrium  $^{[4]}B \leftrightarrow ^{[3]}B$  is shifted to the right. Since the formation  
26 of  $AlPO_4$  units is not a satisfying explanation, one may suggest that when only one dopant ( $P_2O_5$  or

Al<sub>2</sub>O<sub>3</sub>) is introduced, it is preferentially present in the phase with which it has an affinity. In the case of the mixed P<sub>2</sub>O<sub>5</sub>/Al<sub>2</sub>O<sub>3</sub> glasses the assumptions made above do not explain the observed tendencies of the IR, XPS and NMR measurements. When approaching the composition  $x = 1.5$  the number of nbOs should be reduced compared to the aluminate-rich phase, and should be increased compared to the phosphate-rich phase. That is why it is possible that phosphate and aluminate group interact at the frontier of the silicate and borate phase domains, thus locally affecting both networks. Other hypothesis may also explain some features, such as the formation of alumina-rich domains, as suggested by Monteil et al. by molecular dynamics [51]. Correlative multi-nuclei NMR studies may help solving these issues.

#### 4.3. Influence of the structure on the emission properties

As seen in Fig. 2b-e and 4, the addition of Al<sub>2</sub>O<sub>3</sub> and/or P<sub>2</sub>O<sub>5</sub> has a strong impact on the absorption and emission properties of Er<sup>3+</sup> ions. The changes in the shapes and intensities of these bands tend to indicate that the Al and P atoms most probably participate to the second coordination shell around the Er<sup>3+</sup> ions, while being progressively introduced in the borosilicate glass matrix. Similar changes in the surrounding environment of Er<sup>3+</sup> after the introduction of P<sub>2</sub>O<sub>5</sub> in sodium aluminosilicate glasses have been reported elsewhere [52]. The decrease of the absorption cross-sections at 980 nm and of the absorption intensity at 1530 nm (Fig. 2d and 2e) traduces a lowering of the 4f-4f transitions probabilities when  $x$  increases from 0 to 3. Therefore the Er<sup>3+</sup> site is expected to be less non-centrosymmetric with the progressive addition of Al<sub>2</sub>O<sub>3</sub> at the expense of P<sub>2</sub>O<sub>5</sub>. As the Pauling electronegativity of P (2.19) is higher than that of Al (1.61) [53], it is reasonable to think that the strong P–O bonds have a higher influence on the Er<sup>3+</sup> site than the Al–O bonds increasing the probability of the 4f-4f transition. It is interesting to notice that the changes in the Er<sup>3+</sup> absorption and emission band at 1530 nm are more pronounced with the addition of P<sub>2</sub>O<sub>5</sub> than with the Al<sub>2</sub>O<sub>3</sub> addition confirming the strong role of phosphorus on the Er<sup>3+</sup> site distortion. The decrease of the relative intensity of the emission band at 1490 nm over the one at 1530 nm

1 when the  $\text{Al}_2\text{O}_3$  concentration increases may be explained by a modification of the electronic  
2 population of the  $^4\text{I}_{13/2}$  sub-levels favoring the sub-level at 1530 nm at the expense of the one at  
3 1490 nm. This is also confirmed by the fact that the glasses with  $x \sim 1$  have a higher emission  
4 intensity at 1530 nm than the glass with  $x = 3$  while having a similar absorption cross-section at 980  
5 nm but a higher OH content. The local maximum of the absorption cross-section for  $x \sim 1.5$  (Fig. 2d  
6 and 2e) is most probably related to the formation of Al–O–P linkages in the network, which are also  
7 believed to have a significant  $\text{Er}^{3+}$  site distorting role. However, while the glass with  $x = 1.5$   
8 exhibits a similar absorption cross-section at 980 nm and a similar OH content that the glass  $x = 0$ ,  
9 the glass  $x = 1.5$  exhibits however a lower emission at 1530nm. This is not fully understood and  
10 still under investigation. The low emission at 1530 nm of the glass with  $x = 3$  can be related to the  
11 high content in hydroxyl groups as seen in Fig. 3, since it is well know that OH hydroxyl groups are  
12 serious quenchers of  $\text{Er}^{3+}$  ions luminescence [54,55]. Theoretical calculations by the Judd-Ofelt  
13 analysis are in progress in order to get a better description of the  $\text{Er}^{3+}$  coordination environment.

14

## 15 5. Conclusion

16 The goal of this study was to evaluate the influence of  $\text{P}_2\text{O}_5$  and  $\text{Al}_2\text{O}_3$  content on the  
17 structure of erbium-doped sodium-borosilicate glasses and also on their physical, thermal, optical  
18 and luminescence properties. The addition of  $\text{P}_2\text{O}_5$  or  $\text{Al}_2\text{O}_3$  at the expense of  $\text{B}_2\text{O}_3$  and  $\text{Na}_2\text{O}$   
19 results in an increase of the polymerization degree of the silicate network while the fraction of  $^{[4]}\text{B}$   
20 increases, with various ratios of neutral and charged  $^{[3]}\text{B}$  species. These changes in the structure  
21 have been related to changes in  $T_g$ ,  $n$ , absorption cross-sections at 1530 nm and 980 nm and also in  
22 the emission at 1530 nm. Al and P are strongly suspected to modify the coordination shell of  $\text{Er}^{3+}$ ,  
23 thus affecting the optical and luminescence properties. To conclude, the present study has  
24 demonstrated the better efficiency of phosphorous rather than aluminium in the declustering process  
25 of erbium ions in sodium borosilicate glasses with a low silica content.

26

## 1    **Acknowledgments**

2            A part of the research leading to these results has received funding from the European Union  
3    Seventh Framework Programme FP7/2007-2013 under grant agreement n°264526 through the  
4    GlaCERCo Marie-Curie ITN project. The Finnish Funding Agency for Technology and Innovation  
5    (TEKES) is acknowledged by nLIGHT for financial support. The Academy of Finland is gratefully  
6    acknowledged for the financial support of J.M.. The help of S. Guastella for the XPS measurements  
7    and of A. Venturella for the FTIR measurements is greatly acknowledged.

## 9    **References**

- 10    [1] B. E. A. Saleh, M. C. Teich, Fundamentals of Photonics, Wiley, New York (1991).
- 11    [2] P. C. Becker, N. A. Olsson, Jay R. Simpson, Erbium-Doped Fiber Amplifiers: Fundamentals  
12    and Technology, Academic Press Inc. (London, 1999) Std..
- 13    [3] A.J. Kenyon, Progress in Quant. Electr., 26 (2002), 225–284.
- 14    [4] S.E. Stokowski, R. A. Saroyan, M. J. Weber, Lawrence Livermore National Laboratory Report  
15    M-095 2 (1981).
- 16    [5] W.J. Miniscalco, J. Lightwave Technol. 9 (1999) 234–250.
- 17    [6] M.M. Bubnov, V.N. Vechkanov, A.N. Gur’yanov, K.V. Zotov, D.S. Lipatov, M.E. Likhachev,  
18    M.V. Yashkov, Inorg. Mat. 45 (2009), 444–449.
- 19    [7] M. J. Weber, J. Non- Cryst. Solids 123 (1990) 208–222.
- 20    [8] S. Jetschke, S. Unger, A. Schwuchow, M. Leich, J. Kirchhof, Opt. Express 16 (2008) 15540.
- 21    [9] S. Sen, R. Rakhmatullin, R. Gubaidullin, A. Pöppl, Phys. Rev. B 74 (2006) 100201.
- 22    [10] M.J.F. Digonnet, Rare-Earth-Doped Fiber Lasers and Amplifiers, Marcel Dekker, New York  
23    (2002).
- 24    [11] K. Arai, H. Namikawa, K. Kumata, T. Honda, Y. Ishii, T. Handa., J. Appl. Phys. (1986)  
25    593430–3436.

- 1 [12] W.F. Du, K. Kuraoka, T. Akai, T. Yazawa, J. Mat. Sci. 35 (2000) 4865.
- 2 [13] E.I. Kamitsos, J.A Kapoutsis, H. Jain, H.S. Hsieh, J. Non-Cryst. Solids, 172 (1994) 31–45.
- 3 [14] K. El-Egili, Physica B 325 (2003) 340–348.
- 4 [15] M. Okuno, N. Zotov, M. Schmucker, H. Schneider, J. Non-Cryst. Solids 351 (2005) 1032–  
5 1038.
- 6 [16] D. Moncke, D. Ehrt, C.-P.E. Varsamis, E.I. Kamitsos, A.G. Kalampounias, Proc. Fifth Int.  
7 Conf. on Borate Glasses, Crystals and Melts Glass Tech.: Eur. J. Glass Sci. Technol. A 47 (2006)  
8 133–137.
- 9 [17] J. Massera, C. Claireaux, T. Lehtonen, J. Tuominen, L. Hupa, M. Hupa, J. Non-Cryst. Solids,  
10 357 (2011) 3623–3630.
- 11 [18] A. Quintas, D. Caurant, O. Majérus, T. Charpentier, J.-L. Dussossoy, Mat. Res. Bull. 44 (2009)  
12 1895–1898.
- 13 [19] M.E. Likhachev, M.M. Bubnov, K.V. Zotov, O.I. Medvedkov, D.S. Lipatov, M.V. Yashkov, A  
14 N Guryanov, Quant. Electr. 40 (2010), 633–638.
- 15 [20] D.J. DiGiovanni, J.B. MacChesney, T.Y. Kometani, J. Non-Cryst. Solids 113 (1989) 58.
- 16 [21] S.G. Kosinski, D.M. Krol, T.M. Duncan, D.C. Douglass, J.B. MacChesney, J.R. Simpson, J.  
17 Non-Cryst. Solids 105 (1988) 45–52.
- 18 [22] E.I. Kamitsos, G.D. Chryssikos, J. Molec. Struct. 247 (1991) 1.
- 19 [23] W. J. Dell, P. J. Bray and S. Z. Xiao, J. Non-Cryst. Solids 58 (1983) 1.
- 20 [24] V.G. Plotnichenko, V.O. Sokolov, V.V. Koltashev, E.M. Dianov, J. Non-Cryst. Solids 306  
21 (2002) 209–226.
- 22 [25] H. Li, P. Hrma, J.D. Vienna, M. Qian, Y. Su, D.E. Smith, J. Non-Cryst. Solids 331 (2003)  
23 202–216.
- 24 [26] S. Liu, Y. Zhang, W. He, Y. Yue, J. Non-Cryst Solids 357 (2011) 3897.
- 25 [27] Y. Yan, A.J. Faber, H. Waal, J. Non-Cryst. Solids 181 (1995) 283.

1 [28] L. Nemec, J. Gotz, J. Am. Ceram. Soc. 53 (1970) 526.

2 [29] S.N. Houde-Walter, P.M. Peters, J.F. Stebbins, Q. Zeng, J. Non-Cryst. Solids 286 (2001)

3 118–131.

4 [30] S.N.B. Bhaktha, B. Boulard, S. Chaussedent, A. Chiappini, A. Chiasera, E. Duval, C.

5 Duverger, S. Etienne, M. Ferrari, Y. Jestin, M. Mattarelli, M. Montagna, A. Monteil, E. Moser, H.

6 Portales, K.C. Vishunubhatla, Opt. Mat. 28 (2006) 1325–1328.

7 [31] N. Ollier, T. Charpentier, B. Boizot, G. Wallez, D. Ghaleb, J. Non-Cryst. Solids 341 (2004) 26

8 [32] A. S. Tenney and J. Wong, J. Chem. Phys. 56 (1972) 5516–5523.

9 [33] R.J. Bell, A. Carnevale, C.R. Kurkjian, G.E. Peterson, J. Non-Cryst. Solids, 35–36 (1980)

10 1185–1190.

11 [34] E.I. Kamitsos, A.P. Patsis, M.A. Karakassides, G.D. Chryssikos, J. Non-Cryst. Solids 126

12 (1990) 52–67.

13 [35] E.I. Kamitsos, A.P. Patsis, G.D. Chryssikos, J. Non-Cryst. Solids, 152 (1993) 246–257.

14 [36] N.M. Vedishcheva, B.A. Shakhmatkin, A.S. Wright, Phys. Chem. Glasses 44 (2003) 191–196.

15 [37] J.E. Shelby, Introduction to Glass Science and Technology, Royal Soc. Chem., 2<sup>nd</sup> Edition

16 (2005).

17 [38] D. Chen, H. Miyoshi, H. Masui, T. Akai, T. Yazawa, J. Non-Cryst. Solids 345–346 (2004)

18 104–107.

19 [39] V. E. Eremyashev, A. A. Osipov, L. M. Osipova, Glass and Ceramics 68 (2011) 205–208.

20 [40] G. Gao, L. Hu, H. Fan, G. Wang, K. Li, S. Feng, S. Fan, H. Chen, Opt. Mat. 32 (2009) 159–

21 163.

22 [41] L. Wondraczek, G. Gao, D. Möncke, T. Selvam, A. Kuhnt, W. Schwieger, D. Palles, E.I.

23 Kamitsos, J. Non-Cryst. Solids 360 (2013) 36–40.

24 [42] G.D. Chryssikos, E. I. Kamitsos, Proc. Int. Symp. Glass Sci. Tech. (1993) Edited by G. D.

25 Chryssikos & E. I. Kamitsos, Greek Glass Federation, Athens, Greece.

- 1 [43] U. Moryc, W.S Ptak, J. Mol. Struct., 511–512 (1999) 241–249.
- 2 [44] D. Möncke, M. Dussauze, E. I. Kamitsos, C.P.E. Varsamis, D. Ehrt, Phys. Chem. Glasses: Eur.
- 3 J. Glass Sci. Technol. B 50 (2009) 229–235.
- 4 [45] Y. D. Yiannopoulos, G. D. Chryssikos, E. I. Kamitsos, Phys. Chem. Glasses 42 (2001)
- 5 164–172.
- 6 [46] Mysen85 B.O. Mysen, D. Virgo, I. Kushiro, Am. Mineral. 70 (1985) 88.
- 7 [47] R.K. Brow, D.R. Tallant, S.T. Myers, C.C. Phifer, J.-Non-Cryst. Solids 191 (1995) 45–55.
- 8 [48] M. Rokita, M. Handke, W. Mozgawa, J. Mol. Struct. 450 (1998) 213.
- 9 [49] M. Rokita, M. Handke, W. Mozgawa, J. Mol. Struct. 555 (2000) 351–356.
- 10 [50] 50 L.D. Pye, V.D. Frechette, N.J. Kreidl, Borate glasses: structure, properties, applications ;
- 11 Plenum Press, New York (1978).
- 12 [51] A. Monteil, S. Chaussedent, G. Alombert-Goget, N. Gaumer, J. Obriot, S.J.L. Ribeiro, Y.
- 13 Messaddeq, A. Chiasera, and M. Ferrari, J. Non-Cryst. Solids 348 (2004) 44.
- 14 [52] J. Ding, Y. Chen, W. Chen, L. Hu, G. Boulon, Chin. Opt. Lett. 10 (2012) 071602.
- 15 [53] J.E. Huheey, E.A. Keiter, R.L. Keiter, Inorganic Chemistry: Principles of Structure and
- 16 Reactivity, 4th edition, HarperCollins, New York, USA (1993).
- 17 [54] Y. Yan, A.J. Faber, H. de Waal, J.-Non-Cryst. Solids 181 (1995) 283–290.
- 18 [55] X. Feng, S. Tanabe, T. Hanada, J. Non-Cryst. Solids 281 (2001) 48.

19

## Table captions

1

2 Table 1. Glass composition, label, glass density, absorption coefficient at  $3500\text{ cm}^{-1}$ , OH group  
3 concentration

4 Table 2. Values of  $R$  ( $= \text{Na}_2\text{O}/\text{B}_2\text{O}_3$ ),  $R'$  ( $= (\text{Na}_2\text{O}-\text{Al}_2\text{O}_3)/\text{B}_2\text{O}_3$ ),  $R^*$  ( $= (\text{Na}_2\text{O}-\text{P}_2\text{O}_5-$   
5  $\text{Al}_2\text{O}_3+2^*\text{AlPO}_4)/\text{B}_2\text{O}_3$ ), and  $N_3$ ,  $N_4$ ,  $Q^3$  and  $Q^4$  fractions calculated by the Dell-Bray-Xiao (DBX)  
6 model before and after modification.

7



1

Table 1

2

										3	
x	SiO <sub>2</sub> (mol%)	Na <sub>2</sub> O (mol%)	B <sub>2</sub> O <sub>3</sub> (mol%)	Er <sub>2</sub> O <sub>3</sub> (mol%)	P <sub>2</sub> O <sub>5</sub> (mol%)	Al <sub>2</sub> O <sub>3</sub> (mol%)	[Er <sup>3+</sup> ] (×10 <sup>19</sup> ions.cm-3)	$\rho$ (g.cm <sup>-3</sup> )	$\alpha$ (cm <sup>-1</sup> )	[OH] (×10 <sup>19</sup> ions.cm <sup>-3</sup> )	4
											5
								(± 0.05)	(± 5 %)	(±5%)	6
							(±5%)				
	50	21.82	28.06	0.12			5.81	2.46	3.53	4.34	7
0	50	20.51	26.36	0.12	3	0	5.31	2.47	5.08	6.25	8
0.5	50	20.51	26.36	0.12	2.5	0.5	5.31	2.46	7.95	9.77	9
1	50	20.51	26.36	0.12	2	1	5.27	2.44	8.36	10	10
1.18	50	20.51	26.36	0.12	1.82	1.18	5.27	2.43	5.36	6.59	11
1.34	50	20.51	26.36	0.12	1.66	1.34	5.28	2.43	5.46	6.71	12
1.5	50	20.51	26.36	0.12	1.5	1.5	5.31	2.45	4.91	6.04	
1.67	50	20.51	26.36	0.12	1.33	1.67	5.31	2.44	5.09	6.26	
2	50	20.51	26.36	0.12	1	2	5.30	2.43	4.93	6.05	
2.5	50	20.51	26.36	0.12	0.5	2.5	5.35	2.45	6.50	7.98	
3	50	20.51	26.36	0.12	0	3	5.31	2.43	6.37	7.82	

1

Table 2

2

					DBX model				Modified DBX model			
x(Al <sub>2</sub> O <sub>3</sub> )	R	K	R'	R*	N <sub>3</sub>	N <sub>4</sub>	Q <sup>3</sup>	Q <sup>4</sup>	B <sub>3</sub>	B <sub>4</sub>	Q <sup>3</sup>	Q <sup>4</sup>
					(%)	(%)	(%)	(%)	(%)	(%)	(%)	(%)
Matrix	0.78	1.78	0.78	0.78	0.39	0.61	18.7	81.3	0.39	0.61	18.7	81.3
0	0.78	1.90	0.78	0.66	0.38	0.62	16.8	83.2	0.38	0.62	4.8	95.2
0.5	0.78	1.90	0.76	0.70	0.38	0.62	14.8	85.2	0.38	0.62	8.8	91.2
1	0.78	1.90	0.74	0.74	0.38	0.62	12.8	87.2	0.38	0.62	12.8	87.2
1.18	0.78	1.90	0.73	0.75	0.38	0.62	12.1	87.9	0.38	0.62	14.2	85.8
1.34	0.78	1.90	0.73	0.77	0.38	0.62	11.4	88.6	0.38	0.62	15.5	84.5
1.5	0.78	1.90	0.72	0.78	0.38	0.62	10.8	89.2	0.38	0.62	16.8	83.2
1.67	0.78	1.90	0.71	0.77	0.38	0.62	10.1	89.9	0.38	0.62	15.4	84.6
2	0.78	1.90	0.70	0.74	0.38	0.62	8.8	91.2	0.38	0.62	12.8	87.2
2.5	0.78	1.90	0.68	0.70	0.38	0.62	6.8	93.2	0.38	0.62	8.8	91.2
3	0.78	1.90	0.66	0.66	0.38	0.62	4.8	95.2	0.38	0.62	4.8	95.2

3

4

## Figure captions

Fig. 1. (a) Refractive index ( $n_{1312}$ ) at 1312 nm and (b) Glass transition temperature ( $T_g$ ) versus  $x$  (Inset:  $T_x - T_g$  difference. For the matrix glass, no crystallization peak was detected). Solid line is a guide for the eye.

Fig. 2. (a) UV-visible-IR absorption spectrum of the Er-doped borosilicate matrix glass. Absorption cross-section spectra at (b) 980 nm and (c) 1530 nm corresponding respectively to the  $^4I_{15/2} \rightarrow ^4I_{11/2}$  and  $^4I_{15/2} \rightarrow ^4I_{13/2}$  transitions (Insets of (b) and (c): normalized spectra), (d) Evolution of the absorption cross-section at 980 nm versus  $x$  and (e) Absorption peak integral  $A^{Abs}(1530)$  at 1530 nm versus  $x$ . Solid line is a guide for the eye.

Fig. 3. IR absorption spectra of some Er-doped borosilicate glasses with various contents of  $P_2O_5$  and  $Al_2O_3$  in the 3000–4000  $cm^{-1}$  range.

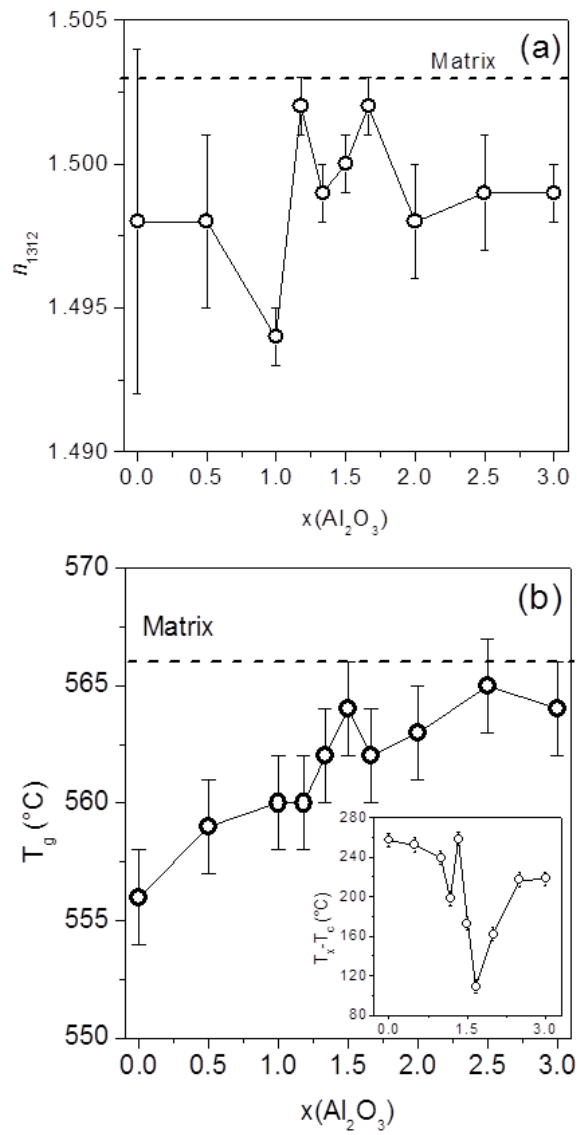
Fig. 4. (a) Emission spectra of some Er-doped borosilicate glasses with various contents of  $P_2O_5$  and  $Al_2O_3$  ( $\lambda_{exc} = 980$  nm) (Inset: normalized spectra) and (b) Emission integral  $A^{Em}(1530)$  at 1530 nm versus  $x$ . Solid line is a guide for the eye.

Fig. 5. Normalized IR reflexion spectra of the glasses (matrix,  $x = 0, 1.5$  and  $3$ ).

Fig. 6. (a) Normalized XPS Si2p spectra of Er-doped borosilicate glasses with various contents of  $P_2O_5$  and  $Al_2O_3$  and (b) Si2p binding energy versus  $x$ . Solid line is a guide for the eye.

- 1 Fig. 7. (a)  $^{11}\text{B}$  MAS NMR spectra of the glasses matrix,  $x = 0, 1.5$  and  $3$ , (b) Evolution of the  $^{13}\text{B}$   
2 and  $^{14}\text{B}$  as a function of  $x$ . Solid line is a guide for the eye.  
3  
4 Fig. 8. Evolution of the silicate fractions ( $Q^3$  and  $Q^4$ ) calculated from the Dell-Bray-Xiao model  
5 before and after modification

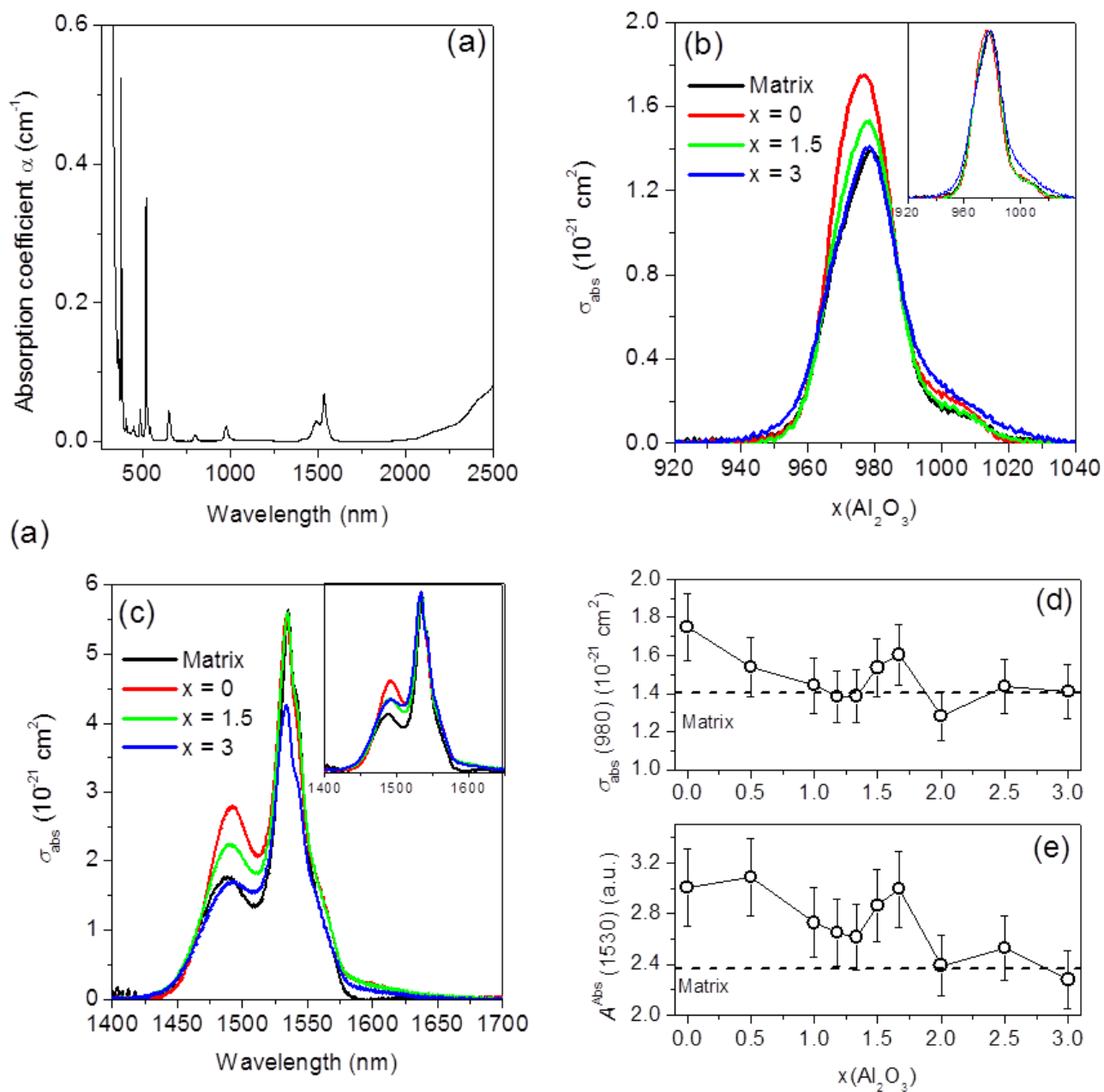
1

**FIG. 1**

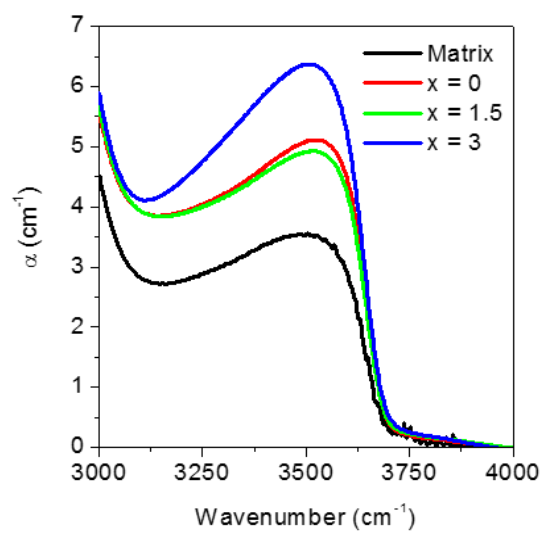
2

3

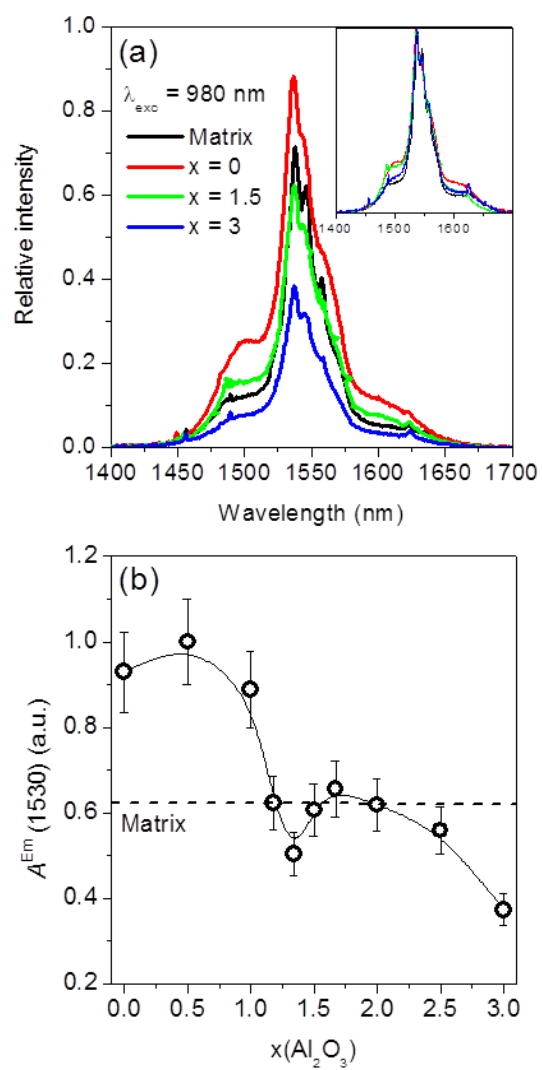
**FIG. 2**



**FIG. 3**

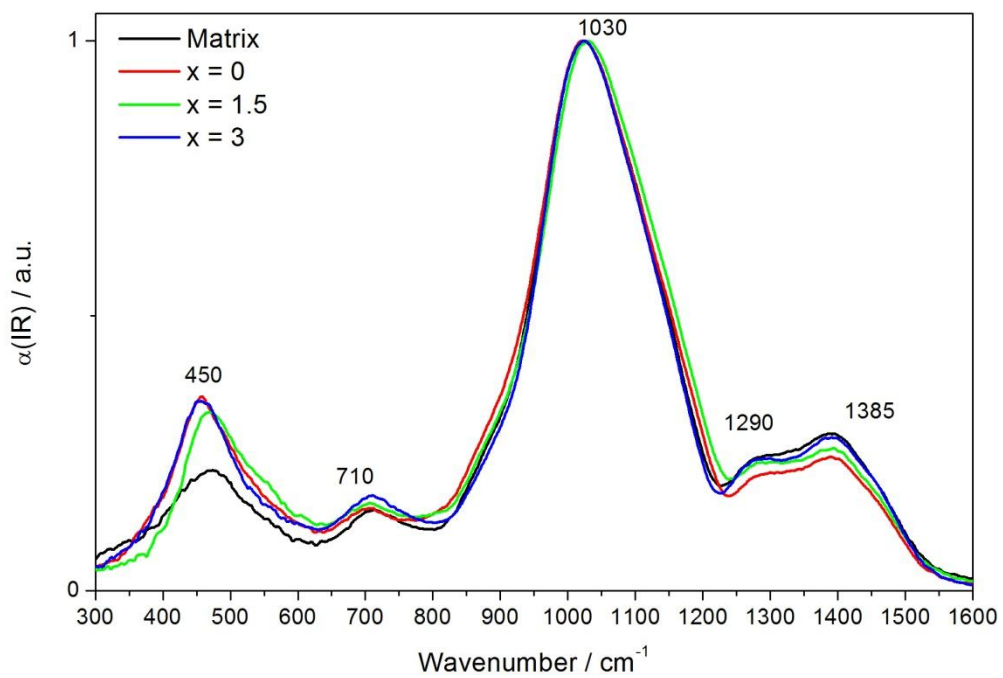


**FIG. 4**





1

**FIG. 5**

2

**FIG. 6**

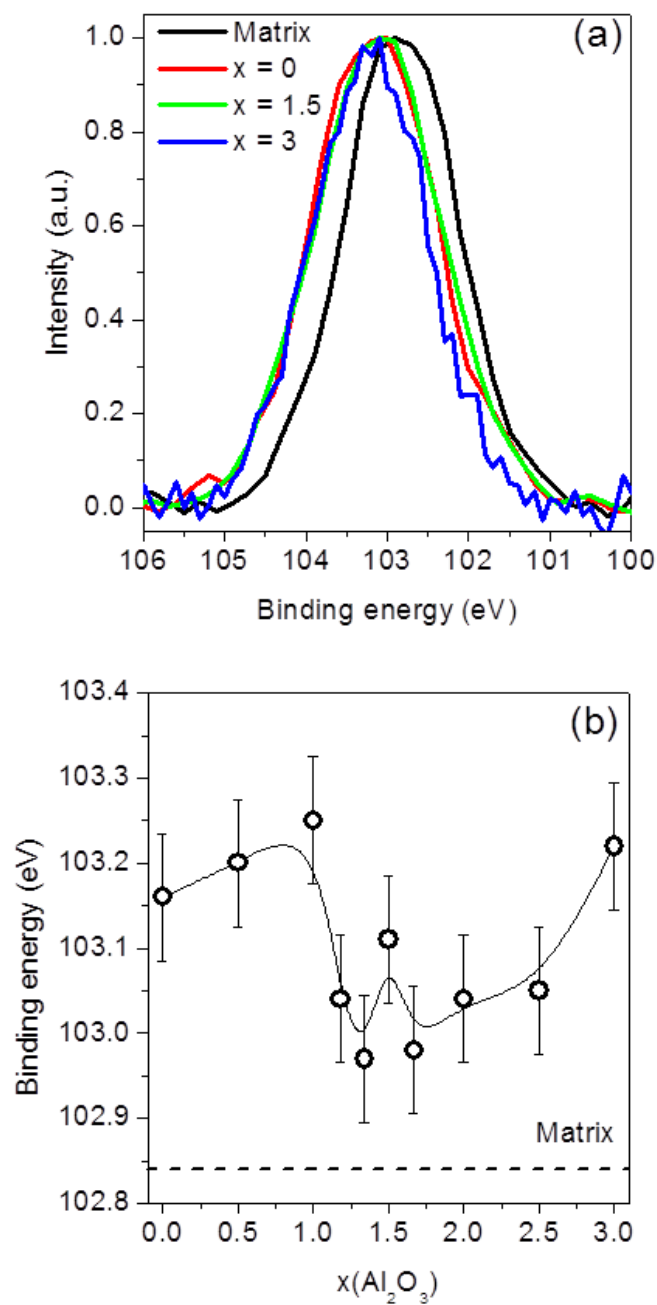


**FIG. 7**

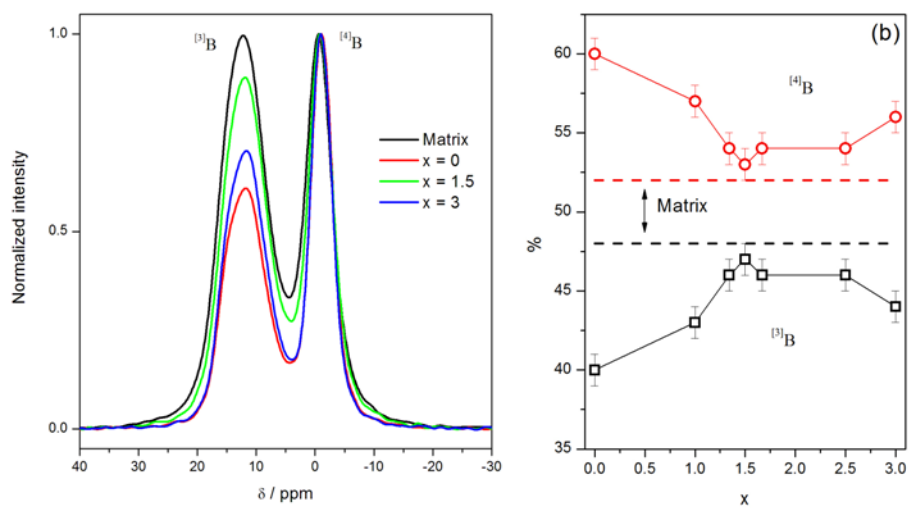


FIG. 8

